NANO LETTERS

Letter

pubs.acs.org/NanoLett

Super-Dispersive Off-Axis Meta-Lenses for Compact High Resolution Spectroscopy

M. Khorasaninejad,*,† W. T. Chen,† J. Oh,†,‡ and F. Capasso*,†

†Harvard John A. Paulson School of Engineering and Applied Sciences, Harvard University, Cambridge, Massachusetts 02138, United States

‡University of Waterloo, Waterloo, Ontario N2L 3G1, Canada

Supporting Information

ABSTRACT: Metasurfaces have opened a new frontier in the miniaturization of optical technology by allowing exceptional control over the wavefront. Here, we demonstrate off-axis meta-lenses that simultaneously focus and disperse light of different wavelengths with unprecedented spectral resolution. They are designed based on the geometric phase via rotated silicon nanofins and can focus light at angles as large as 80°. Due to the large angle focusing, these meta-lenses have superdispersive characteristics (0.27 nm/mrad) that make them capable of resolving wavelength differences as small as 200 pm in the telecom region. In addition, by stitching several meta-lenses together, we maintain a high spectral resolution for a wider wavelength range. The meta-lenses have measured efficiencies as high as 90% in the wavelength range of 1.1 to 1.6 μm. The planar and compact configuration together with high spectral resolution of these meta-lenses has significant potential for emerging portable/wearable optics technology.

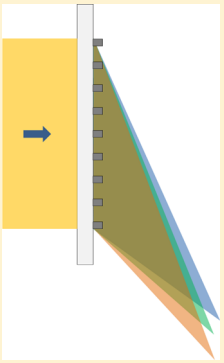

KEYWORDS: *Metasurface, off-axis meta-lens, superdispersive elements, spectroscopy*

Metasurfaces can provide unique solutions to realize complex optical systems in a compact and planar configuration.[1−24] Some major developments have been made in the metasurface field by demonstrating various optical components such as lenses,[2,5,8,12,27] holograms,[13−16,28] and gratings.[17−20] In addition, versatile polarization control devices[19−24,29] have been realized, and it has been envisioned to perform mathematical operations[25,26] using metasurfaces.

Portable/wearable optics for personal health care and environmental monitoring[30−33] is one of the areas where metasurfaces can have a major impact. Spectroscopy is a necessary tool to fulfill this goal since it provides fast turnaround time and high sensitivity. In a conventional spectrometer, a relatively long propagation distance is required to sufficiently separate different wavelengths for high spectral resolution. This requirement makes most spectrometers bulky. Although miniaturized spectrometers are available, their resolution is usually limited to nanometers (∼5−10 nm) in the telecom region.[33,34] Spectral resolution can be improved by integrating a band-pass filter array on top of the camera's pixels.[35,36] However, in addition to complex fabrication, each integrated filter discards light outside its band-pass range making this approach significantly inefficient. In this paper, we demonstrate efficient superdispersive meta-lenses in the telecom range capable of resolving wavelength differences down to 200 pm. This is accomplished by focusing at large angles resulting in a highly dispersive response.

The building blocks of our meta-lenses are silicon nanofins.[29] To focus incident light at an angle α (Figure 1a), secondary waves emerging from each nanofin must arrive at the focal point in-phase. Considering the nanofin at the center of the meta-lens ($x = 0, y = 0$) as the reference, the phase delay due to the difference in optical paths between the nanofin at position (x, y), and the reference can be written as

$$\begin{cases} \varphi_{\mathrm{d}}(x, y) = \dfrac{2\pi}{\lambda_{\mathrm{d}}}\left(\sqrt{(x - x_f)^2 + (y - y_f)^2 + z_f^2} - f\right) \\ f = \sqrt{x_f^2 + y_f^2 + z_f^2} \end{cases} \quad (1)$$

where λ_{d} is the design wavelength and f is the focal length, that is, the distance from the center nanofin to the focal point. To achieve constructive interference and form a focal spot, the above propagation phase difference must be compensated by a phase shift $\varphi_{\mathrm{nf}}(x,y)$ imparted by the nanofin at location (x, y). Therefore, φ_{nf} satisfies the condition $\varphi_{\mathrm{nf}}(x,y) = -\varphi_{\mathrm{d}}(x,y)$. Based on the geometric phase concept,[37,38] this can be accomplished via rotation of the nanofins by an angle $\theta_{\mathrm{nf}}(x,y)$ (Figure S1 of Supporting Information (SI)) which introduces a phase shift $\varphi_{\mathrm{nf}}(x,y) = 2\theta_{\mathrm{nf}}(x,y)$ for right-handed circularly polarized illumination.[2,29,39] Therefore, each nanofin at (x, y) should be rotated by an angle:

$$\theta_{\mathrm{nf}}(x, y) = \frac{\pi}{\lambda_{\mathrm{d}}}\left(f - \sqrt{(x - x_f)^2 + (y - y_f)^2 + z_f^2}\right) \quad (2)$$

Received: March 13, 2016
Revised: April 19, 2016
Published: April 27, 2016

DOI: 10.1021/acs.nanolett.6b01097
Nano Lett. 2016, 16, 3732−3737

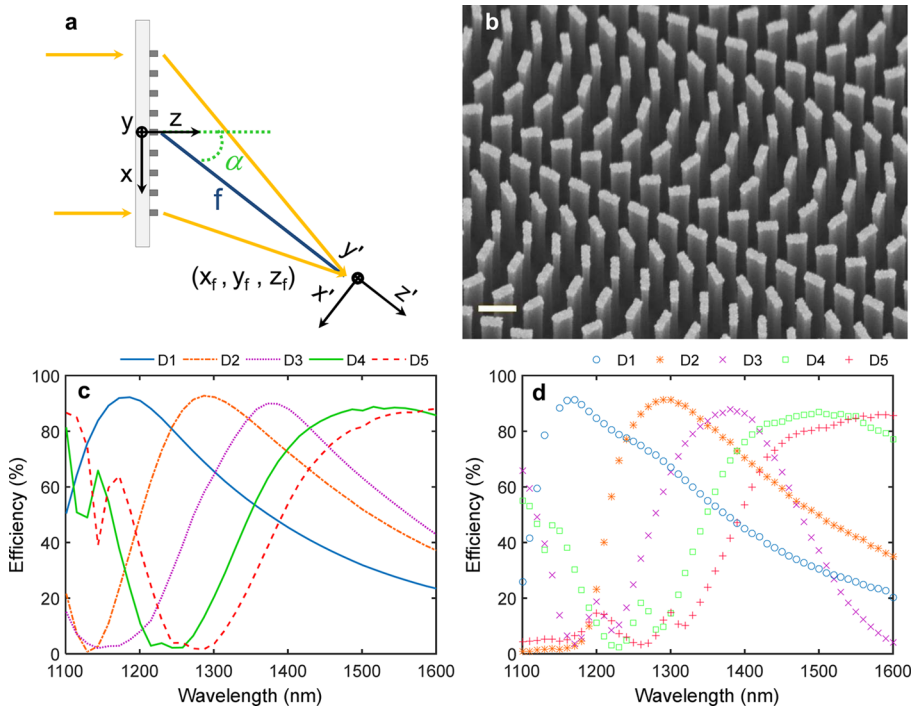

Figure 1. Off-axis meta-lens. (a) Schematic diagram showing the coordinates of the meta-lens. Each nanofin at $(x, y, z = 0)$ compensates for the phase delay associated with the optical path difference relative to the reference optical path (blue line). The latter is defined as the distance from the center nanofin located at $(x = 0, y = 0, z = 0)$ to the focal line $(x = x_f, y = y_f, z = z_f)$. (b) Scanning electron micrograph of the meta-lens. Each nanofin has a width W = 120 nm, length L = 300 nm, and height H = 1500 nm. Nanofins are arranged in a square lattice with a center-to-center distance of 500 nm. Scale bar: 600 nm. (c) Simulation result of the conversion efficiencies under circularly polarized light illumination. The wavelength where maximum efficiency occurs can be adjusted by tuning the nanofins' widths and lengths. There are five designs (D1−D5). For D1−D5, the widths and lengths of the nanofins are W_1 = 90 nm and L_1 = 290 nm, W_2 = 115 nm and L_2 = 300 nm, W_3 = 180 nm and L_3 = 290 nm, W_4 = 105 nm and L_4 = 410 nm, and W_5 = 115 nm and L_5 = 420 nm, respectively. The nanofin heights of all designs are H = 1500 nm. (d) Measured efficiencies of these meta-lenses agree with simulation results. All experiments were performed with circularly polarized light and all meta-lenses in this figure focus at the angle $\alpha = 30°$.

We note that for a meta-lens functioning as a cylindrical lens, φ_{nf} is not a function of y and simplifies to

$$\varphi_{nf}(x) = \frac{2\pi}{\lambda_d}\left(f - \sqrt{(x - x_f)^2 + z_f^2}\right) \quad (3)$$

Using eq 3, we design a lens that focuses light into a line at an angle $\alpha = \sin^{-1}\left(\frac{x_f}{f}\right)$ with a focal length $f = \sqrt{x_f^2 + z_f^2}$. Figure 1b shows the scanning electron micrograph (SEM) of a fabricated meta-lens. Details of the fabrication can be found in ref 29. Nanofin parameters were optimized using the three-dimensional finite difference time domain (FDTD) method from Lumerical Inc. The maximum conversion efficiency for circular polarization occurs when the nanofins act as half-waveplates.[29] As shown in Figure 1c, the wavelength λ_d where the conversion efficiency peaks can be adjusted by modifying the nanofins' parameters, specifically its length and width (Figure S1 of SI). Then, we characterized the meta-lenses using the measurement setup shown in Figure S2 of SI (also see Methods). Efficiencies as high as 90% were obtained (Figure 1d) in agreement with the simulations in Figure 1c. The off-axis angle α affects the efficiency as shown in Figure S3. Both simulations and experiments were performed with circularly polarized light.

As with any other lens, eq 3 shows that the required meta-lens phase profile is wavelength dependent. Due to chromatic aberration, by changing the wavelength, the focal line moves. For on-axis focusing, due to the symmetric nature of its phase profile, the focal line shifts only along the focusing axis. For an off-axis lens, changing the wavelength results in an additional lateral shift of the focal line. This is experimentally observed for our off-axis meta-lens with f = 5 mm, NA = 0.1, $\alpha = 45°$, and λ_d = 1550 nm. Figure 2a shows the focal line shifting along the x'-axis as the wavelength is changed. No displacement along the y'-axis is observed which is expected due to the absence of a phase gradient along the y-axis. This dispersive behavior can be described based on the generalized Snell's laws of refraction.[4] The phase gradient $\left(\frac{d\varphi_{nf}(x)}{dx}\right)$ at the surface of the meta-lens (eq 3) is a function of x. That is to say, at each position x, the meta-lens deflects a portion of the normally incident light by the angle $\gamma(x)$:

$$\sin(\gamma(x)) = \frac{\lambda}{2\pi}\frac{d\varphi_{nf}(x)}{dx} \quad (4)$$

where λ is the incident wavelength. Substituting eq 3 into eq 4, the lateral displacement $(\Delta x')$ of the focal line due to the wavelength change is calculated and shown as the black dashed line in Figure 2a, which follows the experimental results. *This dispersive characteristic can be utilized to resolve the incident wavelength with high precision.* Figure 2b shows that a high spectral resolution of 3 nm is achieved at the design wavelength. This spectral resolution is achieved by combining a highly dispersive lens design with tight focusing down to wavelength-scale lines. We note that the spectral resolution and

DOI: 10.1021/acs.nanolett.6b01097
Nano Lett. 2016, 16, 3732−3737

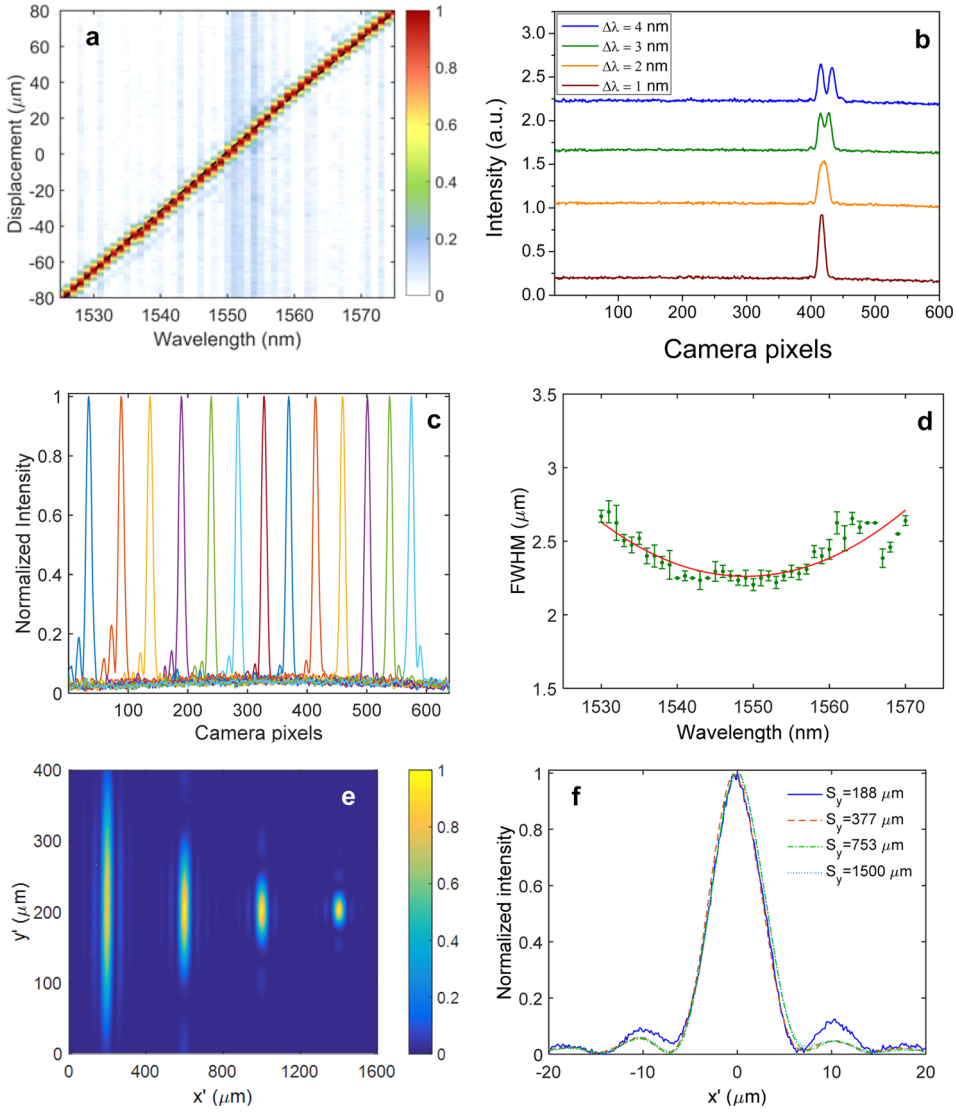

Figure 2. Spectral resolution of an off-axis meta-lens. (a). Displacement of the focal line along the x'-axis (normal to the focal axis) as a function of wavelength. Color-map and dashed line show the experimental results and theoretical prediction, respectively. Any vertical cut of the color-map image is the intensity profile of the meta-lens at the focal length along the x'-axis. For sake of better comparison, we just show a portion of the measured wavelength range. Figure S4 of SI shows the displacement as a function of wavelength for the entire range of measured wavelengths. This meta-lens has focal length f = 5 mm, focusing angle α = 45°, and dimensions of 1.5 mm × 1.5 mm. (b) Superposition of two beam profiles (along the x'-axis at the focal distance) of wavelengths λ_d = 1550 nm and λ = 1550 nm + $\Delta\lambda$. The wavelength difference between the two beams is noted in the inset. A wavelength difference as small as 3 nm is resolved. Camera pixels represent the lateral displacement along x'-axis. (c) Measured intensity profile at focal distance on camera for different wavelengths. Far left curve is the measured focal line profile at 1470 nm wavelength. Wavelength increases by a step of 10 nm from left to right. (d) FWHMs of the beam at the focal line as a function of wavelength for the meta-lens with f = 1.5 mm and α = 45°. (e) The meta-lenses with phase profiles along both the x- and y-axes. This figure shows the measured focal spots of four meta-lenses in the x'-y' plane normal to the focal axis with different meta-lens dimensions along the y-axis (188 μm, 377 μm, 753 μm, and 1500 μm, from left to right). The dimension of all meta-lenses along x-axis is 1.5 mm. (f) Measured intensity profile at focal distance along the x'-axis for four meta-lenses in part e. The experimentally achieved beam sizes are not affected by extra focusing along the y'-axis. For all designs, nanofins have width W = 105 nm, length L = 410 nm, height H = 1500 nm, and center-to-center distance of 500 nm.

focusing (Figure 2c) is maintained over a 120 nm-wide bandwidth, which is within our tunable laser's limit.

The ability to precisely resolve wavelengths at a few millimeters away from the meta-lens offers great potential to implement a supercompact and high-resolution spectrometer. There are three major factors that determine the spectral resolution ($\delta\lambda$) of our meta-lens: focal length (f), focusing angle (α), and numerical aperture (NA). The NA determines the minimum resolvable wavelength difference in the focal plane based on the Rayleigh criterion ($\frac{0.61\lambda}{\mathrm{NA}}$). By substituting eq 3 in to eq 4 and calculating the reciprocal linear dispersion of the meta-lens ($\frac{\Delta\lambda}{\Delta r}$) at its center, x = 0, we will have

$$\frac{\Delta\lambda}{\Delta r} = \frac{\Delta\lambda}{f\Delta\alpha} = \frac{\Delta\lambda}{f\left\{\sin^{-1}\left[\left(1+\frac{\Delta\lambda}{\lambda_d}\right)\sin(\alpha)\right]-\alpha\right\}} \quad (5)$$

where $\Delta\alpha$ is the change in the focusing angle due to a small change of the incident wavelength ($\Delta\lambda$). The spectral resolution of the meta-lens is then given by

DOI: 10.1021/acs.nanolett.6b01097
Nano Lett. 2016, 16, 3732−3737

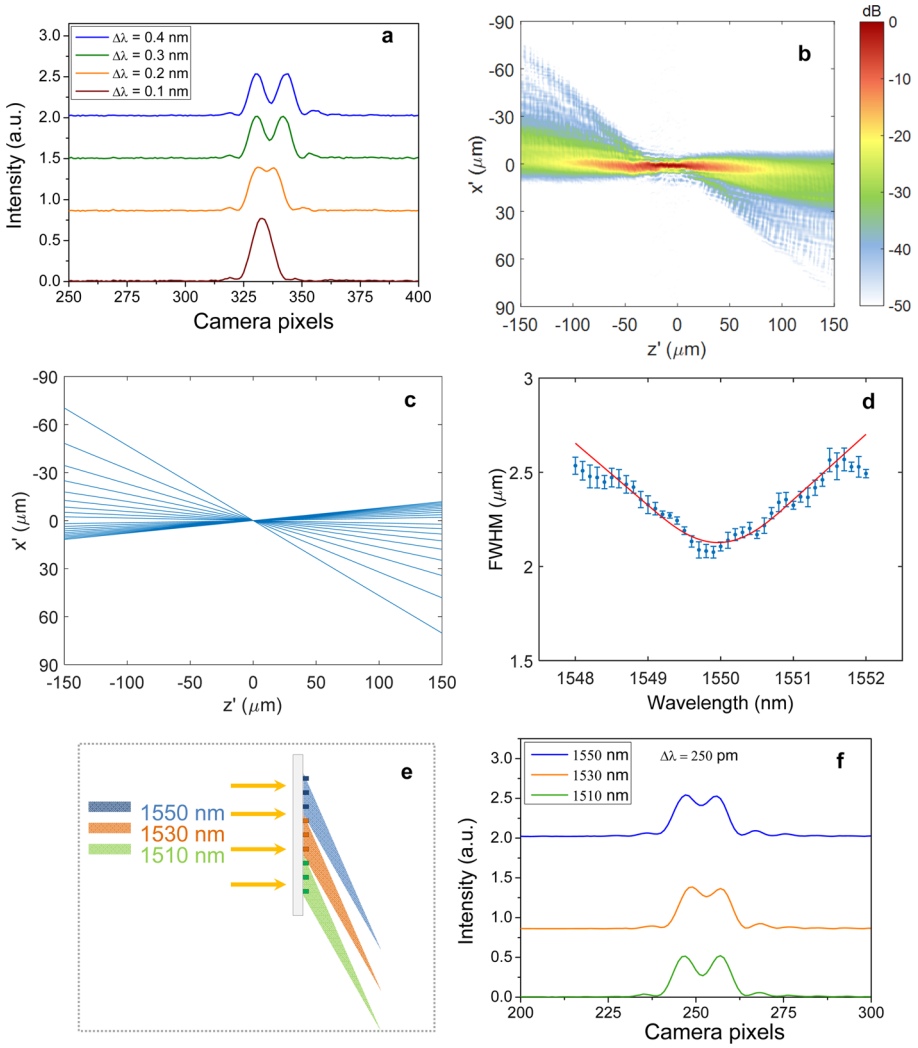

Figure 3. High spectral resolution by focusing at extreme angles. (a) Superposition of two beam profiles along the x'-axis at the focal line. Wavelength differences between the two beams are noted in the legend at the design wavelength λ_d = 1550 nm. A wavelength difference as small as 200 pm is resolved. The meta-lens dimensions are 1 cm along the x-axis and 250 μm along the y-axis. Focal length and angle are 6.1 mm and 80°, respectively. (b) Measured point spread function (PSF) of the meta-lens. Color-map shows experimentally measured intensity in dB units. (c) Simulated PSF using ray-tracing method. (d) Full-width at half-maximum (fwhm) of the focal line versus wavelength. There is trade-off between high spectral resolution and the wavelength range in which the spectral resolution is preserved. By moving from the design wavelength, the focal line broadens. Solid line is to guide the eyes. Measured fwhm at λ = 1550 nm is very close to the theoretical diffraction-limited focal line (fwhm = λ/(2NA) = 2.2 μm, NA = 0.35). (e) Bandwidth in which the spectral resolution is preserved can be extended by stitching several meta-lenses together so that each of them covers a bandwidth of interest without interfering with other bandwidths. This can be achieved by focusing the light in both x- and y-axis (Figure 2e). (f) Superposition of two beam profiles along the x'-axis at the focal length, for each of the three meta-lens stitched together with design wavelengths λ_d = 1510, 1530, and 1550 nm. For all cases nanofins have a width W = 105 nm, length L = 410 nm, height H = 1500 nm, and center-to-center distance of 500 nm.

$$\delta\lambda = \frac{\Delta\lambda}{f\left\{\sin^{-1}\left[\left(1+\frac{\Delta\lambda}{\lambda_d}\right)\sin(\alpha)\right]-\alpha\right\}} \times \frac{0.61\lambda}{NA} \quad (6)$$

Based on this equation, the theoretical spectral resolution is 2.9 nm in agreement with the experimental result in Figure 2b. It is worth noting that the pixel size of the camera also affects the spectral resolution, but it is negligible here (see Methods).

In a conventional grating-based spectrometer, one cannot reduce the distance between the grating and the detector without sacrificing spectral resolution. In a meta-lens-based spectrometer, the resolution can be held constant while making the focal length shorter, which is essential for an ultracompact instrument, by appropriately increasing the NA. In order to demonstrate this, we designed another meta-lens with the same off-axis angle (α = 45°) as the previous meta-lens but with a reduced focal length f = 1.5 mm and an increased NA = 0.35. The higher NA requires modifying the hyperbolic phase profile eq 3 to account for the different focal length so that the fwhm of the focal line is reduced to ~1.4λ (Figure 2d) compared to 4λ of the previous meta-lens. At the design wavelength, the spectral resolution of 3 nm is maintained. However, the trade-off is that for wavelengths away from the design, the spectral resolution is reduced. For example, at wavelengths of 1530 and 1570 nm, a spectral resolution of 3.5 nm is achieved. This reduction is the result of chromatic aberration, which is more pronounced for a higher NA meta-lens. This is evident from Figure 2d where the focal line widens away from the design wavelength. Focal length as a function of wavelength is also measured and shown in Figure S5 of SI.

DOI: 10.1021/acs.nanolett.6b01097
Nano Lett. 2016, 16, 3732−3737

By applying a lens phase profile also along the y-axis, one can focus light into a spot as shown by the experimental results of four meta-lenses in Figure 2e. In addition, this figure shows that the size of the focal spot along the y'-axis can be controlled by simply adjusting the dimension of the meta-lens along the y-axis. The dimension of all four meta-lenses along the x-axis is fixed yielding the same focal spot size along the x'-axis (Figure 2f) which determines the spectral resolution. This design freedom can potentially reduce the size of a required detector array for a spectrometer and at the same time enhance the signal-to-noise ratio by increasing the intensity of the signal per pixel.

The spectral resolution can be further improved by increasing the focusing angle. The larger the angle, the stronger the dispersion (eq 5). Figure 3a shows that wavelengths separated by 200 pm can be resolved using a meta-lens focusing at $\alpha = 80°$ with $f = 6.1$ mm and NA = 0.35. The angular dispersion of this meta-lens is 0.27 nm/mrad, which is unattainable using blazed gratings due to the shadow effect.[40] We also measured the point spread function (PSF) of this meta-lens (Figure 3b). This measurement was done using the measurement setup shown in Figure S2 of SI where the objective lens, tube lens, and camera are moved along the focal axis (z'-axis) in 500 nm steps to capture the intensity profile in the $x'-y'$ plane. This process is repeated to cover a ± 150 μm range around the focal line ($z' = 0$). The intensity distributions of all captured images are stitched together to form the PSF. Beam profile at the focal distance is also shown in Figure S6 of SI. Due to the large size of the meta-lens (1 cm × 250 μm) and our limited computational resources, it was not possible to simulate the PSF using a full-wave analysis technique. Instead, we use a simple ray-tracing technique in which the angles of the rays were calculated based on eq 4. This calculation is shown in Figure 3c (also see Figure S7), qualitatively agreeing with the measurements in Figure 3b.

As expected, by increasing the spectral resolution, the bandwidth in which it can be preserved is reduced. This can be seen in Figure 3d where the focused beam size becomes larger when going away from the design wavelength of 1550 nm. We can maintain the spectral resolution for a wider wavelength range by stitching several meta-lenses together as shown in Figure 3e. Results of this design are shown in Figure 3f where three meta-lenses, designed for wavelengths of 1510, 1530, and 1550 nm, respectively, are stitched together. Each meta-lens focuses light along both the x'- and y'-axes, preventing overlap between their focused beam. This configuration expands the potential application of the meta-lens to various spectroscopy techniques such as Raman spectroscopy. For example, for a sensor detecting Raman signals, the stitching configuration can yield the maximum resolution in multiple wavelength regimes of interest. This also allows for multispectral spectroscopy with different resolving power and functionalities.

In conclusion, we have demonstrated meta-lenses that can achieve focusing at very large angles resulting in superdispersive characteristics to resolve the incident wavelength in a very compact configuration. Furthermore, by stitching meta-lenses with different design wavelengths, we preserved the spectral resolution for a wider wavelength range with additional potential to improve the signal-to-noise ratio in a spectroscopic system. Due to their birefringent nature, nanofins have been used to distinguish the handedness of light.[29] As a result, these meta-lenses can also enable high-efficiency multispectral and chiral imaging. The applications of these meta-lenses can be extended into the visible range using materials such as gallium phosphide and titanium dioxide, which also have relatively high refractive indices with negligible loss. In particular, since beam size is proportional to wavelength, we expect to improve the spectral resolution by operating at the shorter wavelengths of the visible range.

Methods. *Measurement Setup and Efficiency Characterization.* Meta-lenses were characterized using a custom-built microscope consisting of a fiber-coupled laser source, linear polarizer, quarter-waveplate, and objective lens paired with a tube lens to form an image on an InGaAs camera (OWL 640 SWIR from Raptor Photonics). Schematic diagram of the setup is shown in Figure S2 of SI. For efficiency measurements, we used a supercontinuum laser (SuperK and Select from NKT) with a line width of 15 nm. The efficiency was defined as the ratio of the optical power of the focused beam to the optical power of the incident beam. For the efficiency measurements, the optical power was measured by substituting the InGaAs camera with a near-infrared germanium photodiode (Thorlabs S122C). The incident optical power was measured as the light passing through an aperture (aluminum on glass) with the same size of the meta-lens. For spectral resolution characterization and focused beam profile measurements, the light source was a tunable laser (HP-Agilent, 8168-F) with a line width of 1 pm.

Effect of Pixel Size on Spectral Resolution. The spectral resolution of an off-axis meta-lens is defined as the smallest wavelength difference one can distinguish on a camera. There are three factors that affect the spectral resolution: the NA, the reciprocal linear dispersion of the meta-lens, and the pixel size (D) of the camera used. The reciprocal linear dispersion is determined once the focal length and the focusing angle of a meta-lens are given (eq 5). In our system, since the focal spot is magnified and imaged on a camera, its pixel size determines the number of discrete points in which the two closest focal spots can be digitized. Recalling the Rayleigh criterion, if the pixel size of the camera is large compared to $\frac{0.61\lambda}{\mathrm{NA}} \times \frac{1}{2}$, due to the Nyquist-Shannon sampling theorem, aliasing occurs such that distinguishing the two closest spots becomes impossible. Notice that in order to distinguish two spots at least three pixels are needed. Therefore, the spectral resolution is further limited by the factor $3\frac{D}{M} \times \frac{\Delta\lambda}{\Delta r}$, where D is the pixel size of the camera and M is the magnification of imaging system. The spectral resolution $\delta\lambda$ can then be shown by a simple convolution to be the sum of $\frac{0.61\lambda}{\mathrm{NA}} \times \frac{\Delta\lambda}{\Delta r}$ and $3\frac{D}{M} \times \frac{\Delta\lambda}{\Delta r}$.

The numerical aperture was calculated as $\mathrm{NA} = \sin\left(\frac{\beta}{2}\right)$. The definition of β is provided in Figure S8 of the SI.

■ ASSOCIATED CONTENT

Supporting Information

The Supporting Information is available free of charge on the ACS Publications website at DOI: 10.1021/acs.nanolett.6b01097.

Schematic of a unit cell of the meta-lens, measurement set-ups, simulated efficiencies for different diffraction angles, dispersive characteristics: experiment versus simulation, focal length as a function of wavelength, curve fitting example, ray-tracing for meta-lens designed at $\alpha = 80°$, and the definition of numerical aperture (PDF)

DOI: 10.1021/acs.nanolett.6b01097
Nano Lett. 2016, 16, 3732−3737

AUTHOR INFORMATION

Corresponding Authors

*E-mail: capasso@seas.harvard.edu.

*E-mail: khorasani@seas.harvard.edu.

Author Contributions

M.K. and W.T.C. contributed equally to this work.

Notes

The authors declare no competing financial interest.

ACKNOWLEDGMENTS

This work was supported in part by the Air Force Office of Scientific Research (MURI, grant no. FA9550-14-1-0389), Charles Stark Draper Laboratory (grant no. SC001-0000000959), and Thorlabs Inc. W. T. C. acknowledges a postdoctoral fellowship from Ministry of Science and Technology, Taiwan (104-2917-I-564-058). Fabrication work was carried out in the Harvard Center for Nanoscale Systems (CNS), which is part of the National Nanotechnology Infrastructure Network (NNIN) supported by the National Science Foundation. We thank E. Hu for the supercontinuum laser (NKT "SuperK").

REFERENCES

(1) Yu, N.; Capasso, F. *Nat. Mater.* **2014**, *13*, 139−150.

(2) Lin, D.; Fan, P.; Hasman, E.; Brongersma, M. L. *Science* **2014**, *345*, 298−302.

(3) Schuller, J. A.; Zia, R.; Taubner, T.; Brongersma, M. L. *Phys. Rev. Lett.* **2007**, *99*, 107401.

(4) Yu, N.; Genevet, P.; Kats, M. A.; Aieta, F.; Tetienne, J. P.; Capasso, F.; Gaburro, Z. *Science* **2011**, *334*, 333−337.

(5) Aieta, F.; Kats, M. A.; Genevet, P.; Capasso, F. *Science* **2015**, *347*, 1342−1345.

(6) Lu, F.; Sedgwick, F. G.; Karagodsky, V.; Chase, C.; Chang-Hasnain, C. J. C. *Opt. Express* **2010**, *18*, 12606−12614.

(7) Fattal, D.; Li, J.; Peng, Z.; Fiorentino, M.; Beausoleil, R. G. *Nat. Photonics* **2010**, *4*, 466−470.

(8) Khorasaninejad, M.; Aieta, F.; Kanhaiya, P.; Kats, M. A.; Genevet, P.; Rousso, D.; Capasso, F. *Nano Lett.* **2015**, *15*, 5358−5362.

(9) Monticone, F.; Estakhri, N. M.; Alù, A. *Phys. Rev. Lett.* **2013**, *110*, 203903.

(10) Wang, Q.; Rogers, E. T.; Gholipour, B.; Wang, C.-M.; Yuan, G.; Teng, J.; Zheludev, N. I. *Nat. Photonics* **2015**, *10*, 60−65.

(11) Ni, X.; Emani, N. K.; Kildishev, A. V.; Boltasseva, A.; Shalaev, V. M. *Science* **2012**, *335*, 427−427.

(12) Chen, X.; Huang, L.; Mühlenbernd, H.; Li, G.; Bai, B.; Tan, Q.; Jin, G.; Qiu, C.-W.; Zhang, S.; Zentgraf, T. *Nat. Commun.* **2012**, *3*, 1198.

(13) Chen, W. T.; Yang, K.-Y.; Wang, C.-M.; Huang, Y.-W.; Sun, G.; Chiang, I.-D.; Liao, C. Y.; Hsu, W.-L.; Lin, H. T.; Sun, S. *Nano Lett.* **2014**, *14*, 225−230.

(14) Zheng, G.; Mühlenbernd, H.; Kenney, M.; Li, G.; Zentgraf, T.; Zhang, S. *Nat. Nanotechnol.* **2015**, *10*, 308−312.

(15) Huang, Y.-W.; Chen, W. T.; Tsai, W.-Y.; Wu, P. C.; Wang, C.-M.; Sun, G.; Tsai, D. P. *Nano Lett.* **2015**, *15*, 3122−3127.

(16) Huang, K.; Dong, Z.; Mei, S.; Zhang, L.; Liu, Y.; Liu, H.; Zhu, H.; Teng, J.; Luk'yanchuk, B.; Yang, J. K. W.; Qiu, C.-W. *Laser Photon. Rev.* **2016**, 1−10.

(17) Ribot, C.; Lee, M. S. L.; Collin, S.; Bansropun, S.; Plouhinec, P.; Thenot, D.; Cassette, S.; Loiseaux, B.; Lalanne, P. *Adv. Opt. Mater.* **2013**, *1*, 489−493.

(18) Pors, A.; Nielsen, M. G.; Bozhevolnyi, S. I. *Optica* **2015**, *2*, 716−723.

(19) Khorasaninejad, M.; Capasso, F. *Nano Lett.* **2015**, *15*, 6709−6715.

(20) Li, Z.; Palacios, E.; Butun, S.; Aydin, K. *Nano Lett.* **2015**, *15*, 1615−1621.

(21) Yang, Y.; Wang, W.; Moitra, P.; Kravchenko, I. I.; Briggs, D. P.; Valentine, J. *Nano Lett.* **2014**, *14*, 1394−1399.

(22) Arbabi, A.; Horie, Y.; Bagheri, M.; Faraon, A. *Nat. Nanotechnol.* **2015**, *10*, 937−943.

(23) Khorasaninejad, M.; Zhu, W.; Crozier, K. *Optica* **2015**, *2*, 376−382.

(24) Yin, X.; Ye, Z.; Rho, J.; Wang, Y.; Zhang, X. *Science* **2013**, *339*, 1405−1407.

(25) Chong, K. E.; Staude, I.; James, A.; Dominguez, J.; Liu, S.; Campione, S.; Subramania, G. S.; Luk, T. S.; Decker, M.; Neshev, D. N. *Nano Lett.* **2015**, *15*, 5369−5374.

(26) Silva, A.; Monticone, F.; Castaldi, G.; Galdi, V.; Alù, A.; Engheta, N. *Science* **2014**, *343*, 160−163.

(27) Aieta, F.; Genevet, P.; Kats, M. A.; Yu, N.; Blanchard, R.; Gaburro, Z.; Capasso, F. *Nano Lett.* **2012**, *12*, 4932−4936.

(28) Ni, X.; Kildishev, A. V.; Shalaev, V. M. *Nat. Commun.* **2013**, *4*, 2807.

(29) Khorasaninejad, M.; Crozier, K. B. *Nat. Commun.* **2014**, *5*, 5386.

(30) Tseng, D.; Mudanyali, O.; Oztoprak, C.; Isikman, S. O.; Sencan, I.; Yaglidere, O.; Ozcan, A. *Lab Chip* **2010**, *10*, 1787−1792.

(31) Zhu, H.; Isikman, S. O.; Mudanyali, O.; Greenbaum, A.; Ozcan, A. *Lab Chip* **2013**, *13*, 51−67.

(32) Cetin, A. E.; Coskun, A. F.; Galarreta, B. C.; Huang, M.; Herman, D.; Ozcan, A.; Altug, H. *Light: Sci. Appl.* **2014**, *3*, e122.

(33) Khalil, D.; Sabry, Y.; Omran, H.; Medhat, M.; Hafez, A.; Saadany, B. In *Characterization of MEMS FTIR spectrometer*, SPIE MOEMS-MEMS, 2011; International Society for Optics and Photonics: pp 79300J−79300J-10.

(34) Hamamatsu Mini-Spectrometers Product Page. http://www.hamamatsu.com/eu/en/product/category/5001/4016/index.html (accessed Feb 1, 2016).

(35) Wang, S.-W.; Xia, C.; Chen, X.; Lu, W.; Li, M.; Wang, H.; Zheng, W.; Zhang, T. *Opt. Lett.* **2007**, *32*, 632−634.

(36) Emadi, A.; Wu, H.; de Graaf, G.; Wolffenbuttel, R. *Opt. Express* **2012**, *20*, 489−507.

(37) Pancharatnam, S. *Proc. Ind. Acad. Sci. A* **1956**, *44*, 398−417.

(38) Berry, M. V. *J. Mod. Opt.* **1987**, *34*, 1401−1407.

(39) Bomzon, Z. e.; Biener, G.; Kleiner, V.; Hasman, E. *Opt. Lett.* **2002**, *27*, 285−287.

(40) Hessler, T.; Rossi, M.; Kunz, R. E.; Gale, M. T. *Appl. Opt.* **1998**, *37*, 4069−4079.

DOI: 10.1021/acs.nanolett.6b01097
Nano Lett. 2016, 16, 3732−3737